Canadian Science Publishing | Transactions of the Canadian Society for Mechanical Engineering

# The Effect of Drag Force on The Body Frequencies and The Power Spectrum of a Bladeless Wind Turbine



| | |
|---|---|
| Journal: | *Transactions of the Canadian Society for Mechanical Engineering* |
| Manuscript ID | TCSME-2020-0194.R1 |
| Manuscript Type: | Article |
| Date Submitted by the Author: | 26-Feb-2021 |
| Complete List of Authors: | Maftouni, Negin; Al Zahra University, Mechanical engineering<br>Dehghan Manshadi, Mahsa ; Alzahra University<br>Mousavi, Seyed Milad ; KN Toosi, Mechanical engineering |
| Keywords: | resonance phenomenon; vortex shedding; vortex bladeless wind turbine; oscillation; power spectrum |
| Is the invited manuscript for consideration in a Special Issue? : | Not applicable (regular submission) |
| | |

# The Effect of Drag Force on The Body Frequencies and The Power Spectrum of a Bladeless Wind Turbine

Negin Maftouni[1,*] , Mahsa Dehghan Manshadi[1] and Seyed Milad Mousavi [2]

[1]Department of Mechanical Engineering, Faculty of Engineering, Alzahra University, Tehran, Iran,

[2] Faculty of Engineering, K.N. Toosi University of Technology, Tehran, Iran



*Corresponding author: Negin Maftouni, n.maftouni@alzahra.ac.ir

## Abstract

The new types of bladeless wind turbines and generating electricity using them is one of the most interesting topics for engineering nowadays. Electricity generation using the structural vibration due the resonance phenomenon is the concept behind a vortex bladeless turbine. The present study numerically investigates the effects of the drag force on the body frequency of an oscillating bladeless wind turbine. A 2-D numerical simulation was performed for a cylinder with a semi-circular cross-section in cross-flow in two different cases. The research was conducted for both uncontrolled and controlled oscillating cylinders. The controlling process was performed using a pair of ring magnets as a spring with a variable coefficient. The flow field, vibration, vortex shedding and structural frequencies, and the resonance phenomenon are studied in this research. Finally, the controlled and uncontrolled frequencies of the cylinder are explored, and the power spectrum for various velocities is analyzed in two different states, namely with and without a tuning system. From the results, it can be concluded that the usage of the controlling system in these turbines can greatly regulate the oscillations and increase the frequency value by limiting the vibration amplitude. According to this principle, it can be inferred that increasing the frequency of fluctuations greatly increases the production capacity of these turbines.


**Keywords:** resonance phenomenon; vortex shedding; vortex bladeless wind turbine; oscillation; power spectrum.

# 1. Introduction

Regarding the global interest in implementing new renewable energy resources, there is a strong desire to harvest the wind energy under different conditions. A new idea is using vortex bladeless wind turbines. The flow over a circular cylinder has been an important issue during recent decades. A special case of this physical phenomenon is the single/multiple fixed cylinder, which has an application in heat exchanger tubes. Another case is the single/multiple oscillating cylinders, which is used in power cables and is analyzed using two-way fluid-solid interactions (Two-way FSI). A recent application of this phenomenon is in the vortex bladeless wind turbine. When the flow passes over the body of the turbine, the oscillator, which is fixed to the cantilever rod, will start to oscillate under the effect of the vortex shedding frequency behind the semi-circular cylinder. If the flow frequency takes the natural frequency of the whole body, the structure will resonate, and the pick of electrical power will be produced.

More recent studies have concerned the oscillating circular cylinder with or without damping effects. These studies show the high amplitudes and the low values of system damping in the operational range. The vibration response (Klamo et al., 2006) of the vibrating cylinder, which has a free motion in a flow, was experimentally analyzed in the paper. For results, the authors analyzed the profiles of an elastically mounted cylinder in cross-flow and the influence of the controlling system on the cylinder motion. A study (Placzek et al., 2008) was conducted on an oscillating cylinder subject to free and forced oscillations inside a flow with a low Reynolds number. The analysis was performed by a CFD code with coupling procedure. They have demonstrated the frequency and amplitude of an oscillated cylinder in order to find the effect of a controlling system as a result of study. An experimental investigating was done (Yang et al.,2017) on an oscillating cylinder in a water channel with recirculation flow. Their results show the fact that the flow passed the cylinder modified by the clock wised and counter clock wised rotation of cylinder, generates same outputs. A research was performed (Pham et al., 2010) on the two-dimensional numerical analysis of a cylinder that vibrates transversely in a laminar flow. The study has indicated the effect of flow parameters on the cylinder oscillation response by analyzing the wide range of amplitude and frequency of a cylinder. They conclude that the vibration response changes by increasing the amount of flow parameters. The additional research was made (Jiang et al., 2017) in the field of the computational issues of flow on an oscillating cylinder and the flow features were analyzed as a result. They have demonstrated that flow features are directly affected by the vibration of the structure. Another work (Vandiver, 2012) was done on the flow-induced vibration and the effect of the damping parameters on this vibration. They conclude that the damper system can control the vibration which is caused by flow-induced phenomenon. Knowledge of the

governing relations between magnets helps to design the controlling system. A pair of magnets are used in damping system of vortex bladeless turbine. These magnets help control the vibrations of the system in such a way that they prevent vibrations with large amplitudes. To analyze the spring-damper system for controlling the oscillation and calculate the force between two ring magnets, a paper (Santra et al., 1994) used an adaptive Monte Carlo technique with experimental verification. The work is about a new use of this integration method in calculating the force between the pair of magnet rings. Several studies were performed in the field of harvesting energy using the vortex-induced vibration (VIV) phenomenon. One of these works shows different technologies for harvesting energy via wind energy. Flow-induced vibration was studied specifically in another research. This research investigates the stiffness of a flexible plate at specific Reynolds number (Re=70) (Wang et al., 2020). They have found that the maximum oscillation amplitude takes place at the minimum stiffness and bending deformation has nonlinear manner. Another research (Arionfard and Nishi, 2018) demonstrates the coupling of two circular cylinders and the effect of the vibration on the total body force. Another research studied the deflection of the oscillatory wake that appeared behind a turbine (Bai, 2020). They have introduced a new algorithm to calculate drag and lift forces. In the study that explained the idea of vortex bladeless wind turbine, the system was introduced and the vibration and achieved forces were analyzed (Yanez, 2018).

In the present research, for the first time a comparative study is performed between controlled and uncontrolled systems. Results indicates that it is possible to reduce the amplitude of vibrations due to the drag force on the cylinder occurred by magnetic force of the controller, and also to increase the frequency of the moving part of the turbine. Here a CFD method is implemented to analyze a novel type of bladeless wind turbine with a slightly different curve at the tip of the turbine structure, in compare to the old version. The power spectrum is calculated using Eu dimensionless number. Also variations of St dimensionless number with Re has been considered here.

## 2. Materials and method

### 2.1Geometry and Material

A vortex bladeless wind turbine works on the basis of the vortex-induced vibration (VIV) phenomenon. Generally, the wind direction is variable. The turbine is in the shape of a semi-circular cylinder. There is a decrease in section area when the height increases. Vortex shedding is easily formed for a circular cross-section. It means that the cylinder has a different diameter circle cross-section in its height. The reason is to gain maximum power

efficiency. Figure 1 shows the geometry of a bladeless turbine. D1 and D2 show the dimensions of the cantilever reinforced carbon fiber rod, while D3, D4, and D6 show those of the semi-cylinder body, which is made of the same material. As it can be observed comparing Figures 1 and 2, the curvature at the tip of the turbine in the present study is slightly different from that previous research done with Yanez in 2018.

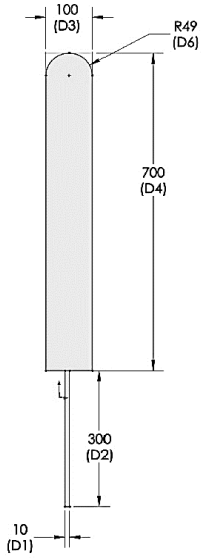


Figure 1. The geometry of the simulated bladeless wind turbine.

The material implemented in this research is reinforced carbon fiber. In general, the properties of carbon fiber, as a bladeless wind turbine body material, include the following: low density, light weight, high tensile modulus and strength, highly directional properties, availability in a continuous form, biocompatibility.

## 2.2Governing Equations

The frequency of vortex shedding is a function of the Strouhal number (St), flow velocity (v), and characteristic length (Φ) (Yanez, 2018);

$$f = \frac{\mathrm{St} \cdot v}{\Phi} \tag{1}$$

The characteristic length of the semi-circular cylinder is obtained from equation (2) and depends on the diameter of the structure. The oscillation of the cylinder is not negligible. It can be proven that the characteristic length is (Yanez, 2018):

$$\Phi = \mathrm{D} + a \cdot X \tag{2}$$

Where (D) is the main diameter of the turbine, (X) is the main amplitude of the oscillating motion, and (a) is the adjustment factor, which depends on a Reynolds number.

In a three-dimensional analysis, the frequency of vortex shedding in any other section of the oscillating body depends on $V_\infty$(y) and X(y), which are the velocity of the airflow and the oscillation amplitude at each height of y (Yanez, 2018);

$$f(y) = \frac{\mathrm{St} \cdot v_\infty(y)}{D(y) + a \cdot X(y)} \tag{3}$$

The parameters are presented in Figure 2;

$$X(y) = \frac{y - \mathrm{L}/2}{\mathrm{H} - \mathrm{L}/2} \cdot \gamma \cdot \mathrm{d} \tag{4}$$

Here, (L) is the flexible and free length of the rod, (d) is the mean diameter of the oscillating part, and (H) is the distance between the anchored point of the rod and the top of the body. The maximum displacement of the top end is ϒ times the lowest diameter of the oscillating body.

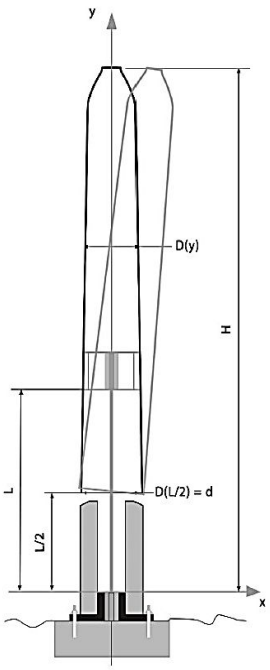


Figure 2. The structure of the vortex bladeless wind turbine (Yanez, 2018).

As the vortex shedding frequency is related to the length of the oscillating part, the following results (Yanez, 2018);

$$D(y) = \mathrm{d} \cdot \frac{v_\infty(y)}{v_\infty\left(\frac{\mathrm{L}}{2}\right)} - a \cdot X(y) \tag{5}$$

The behavior of the oscillating body without a tuning system is similar to a simple spring-damper diagram. If the frequency of the flow is approaching the oscillation frequency, the lock-in range, the structure will resonate.

In other words, in this range, the vortex shedding frequency is shifting toward the natural frequency of the bladeless wind turbine motion and causing vibrations with large amplitudes (Placzek et al., 2020).

The natural frequency of the structure is obtained from equation (6). In the uncontrolled motion of a bladeless wind turbine, m is the mass of the oscillating part which is fixed to the cantilever rod with a specific rigidity, and c is related to the energy losses (Yanez, 2018).

$$f = \frac{1}{2\pi}\sqrt{\frac{k}{m} - \left(\frac{c}{2m}\right)^2} \tag{6}$$

Where m is the mass, which oscillates under the action of the drag force and is connected to a spring of constant elasticity k and a damper of constant c. The controlling system contains two magnets with similar poles that are arranged in a circular array. One of the poles is near the oscillating part, and the other is near the fixed part. The interaction between the magnets with similar poles controls the amplitude of the vibrations. As they approach, the repulsive force between them grows larger. This force is inversely proportional to the square of the average distance between their poles and depends on the amplitude of the oscillations. The magnets behave like a compression spring with non-constant elasticity.

The force between two cylindrical magnets placed next to each other at a suitable distance $x \gg R$ is approximated as;

$$F = \left[\frac{B_0 A^2 (L^2 + R^2)}{\pi \mu_0 L^2}\right]\left[\frac{1}{x^2} + \frac{1}{(x+2)^2} - \frac{2}{(x+L)^2}\right] \tag{7}$$

Here, $B_0$ is the flux density of the magnets (T), which obtained from $B_0 = \frac{\mu_0}{2}M$, A is the area of the magnet surface ($m^2$), L is the length of each magnet (m), R is the radius of the cylindrical magnet (m), and x is the space between the two magnets (m) (Lehner, 2008).

Hence, the frequency of oscillation is increasing with the oscillation amplitude (Yanez, 2018);

$$f(x) = \frac{1}{2\pi}\sqrt{\frac{(k + k'(x))}{m} - \left(\frac{c}{2m}\right)^2} \tag{8}$$

Where k' represents the value of elasticity corresponding to the magnetic repulsion (Yanez, 2018). k' will be obtained from Hooke's Law using the force obtained from Equation (7) and the displacement of the oscillator (oscillation amplitude) (Ugural et al, 2003).

$$F = k'(x) \cdot x \tag{9}$$

The total force exerted on a bladeless wind turbine is called the drag force in the flow direction and is given by;

$$F_D = C_D \frac{1}{2} \rho A V^2 \quad (10)$$

Where ($F_D$) is the drag force, ($C_D$) is the drag coefficient, (ρ) is the density of the air, (A) is the cross-section area which is facing the flow, and (V) is the flow velocity.

The vibration equation for the vertical semi-circular cylinder can be written as;

$$m\ddot{x} + c\dot{x} + kx = F_D \quad (11)$$

Where m is the total mass of the oscillating part, c is the energy loss coefficient, and k is the total elasticity.

When the vortex shedding frequency approaches the natural frequency of the bladeless wind turbine (f), the maximum amplitude of vibration happens. This phenomenon is known as the lock-in range. The oscillation amplitude of a spring-mass system can also be obtained from Equation (12).

$$Y = \frac{F_D}{K}\left[\frac{1}{(1-\eta^2)^2 - (2\xi\eta)^2}\right] \quad (12)$$

where η is the frequency ratio,

$$\eta = \frac{f}{f_{(y)}} \quad (13)$$

Where $f_v$ is the vortex shedding frequency in the Lock-in range, η is equal to 1. Equation (12) will be as follows;

$$Y = \frac{F_D}{2K\xi} \quad (14)$$

This research discusses the effect of a magnetic system controlling the oscillations of a semi-circular cylinder on the maximum vibration amplitude and frequency. Recent research has used this magnetic controlling system, named the tuning system, to control the vibration of bladeless wind turbines by placing two similar poles opposite each other in a circular array. The force between the magnets helps the system to control vibrations and regulates them to a great extent.

## 2.3 Mesh generation and boundary conditions

Mesh generation analysis essentially acquired the number of a sufficient mesh for purposed study. Moreover, three different mesh numbers were generated to simulate a VBT which is presented as Table 1. The computational grid used is a free triangular-mesh type that also satisfies the mesh independency condition. For all calculations, a time step of 0.005 s is used. The computations are carried out for the flow passing over the oscillating bladeless wind turbine with a specific inlet velocity.

Table 1. The information about mesh generation.

| ***Minimum grid size (m)*** | **Simulation time** | **Number of elements** | **Accuracy of analyzed parameter** |
|---|---|---|---|
| *0.05* | 34M 16S | 22541 | 82% |
| *0.005* | 2H 34M 7S | 225229 | 90% |
| *0.004* | 3H 31M 12S | 293476 | 93.6% |
| *0.001* | 8H 58M 10S | 1154301 | 94% |

As presented in Table 1, the numbers of grids increase in mesh blocks to increase the accuracy of the simulation. The criterion to select a minimum grid size is to have high accurate answers due to the least simulation time. Hence, the fine enough triangular grids are chosen including 293476 elements with approximately calculation time of 3.5 hours. Acceptable errors in the purposed bladeless turbine simulations is achieved and the results are independent of the mesh size.

Boundary conditions are defined in such a way that at the boundaries of the wind tunnel walls, except for the inlet and outlet, no-slip condition is assumed for the velocity. The velocity at the inlet is variable and at the outlet the atmospheric pressure is considered. For the bladeless wind turbine body, the slip boundary condition is assumed for velocity. The flow is assumed one dimensional, incompressible and unsteady with constant properties.

## 3. Results and discussion

In this section, the range of amplitude and frequency of an oscillating bladeless wind turbine in a cross-flow field with and without a magnetic controlling system is discussed. Figure 3 shows the vortex shedding and the vortices behind the cylinder.

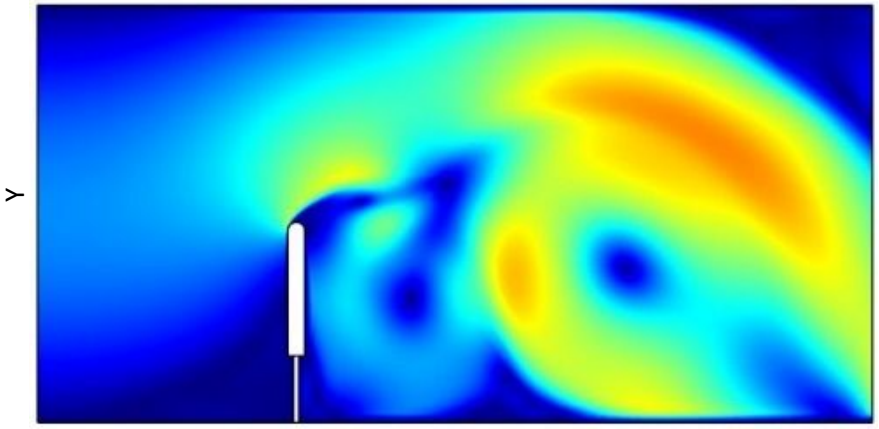

Figure 3. 2D VIV contour of the velocity of vortex shedding which is formed behind the simulated vortex bladeless wind turbine.

The color map shows different colors which means different values of velocity of vortex shedding. It starts from dark blue which introduces the inlet velocity values, to red which defines the vorticities formation velocities. It happens on vortex shedding street.

As mentioned before, one of the most important parameters for fluid simulations is the Strouhal number. This dimensionless number provides the flow frequency, which is related to the vortex shedding frequency behind the bladeless wind turbine. As the flow velocity increases with time, the Reynolds number and the frequency of the vortex shedding will also increase. This procedure continues until the frequency of the vortex shedding near the turbine is equal to the oscillation frequency of the turbine. Simultaneously, the flow and structure frequency will rise, and the final effect on the fluid domain is an increase in the Strouhal number as shown in Figure 4. However, when the velocity increases, the total drag force applied to the semi-circular cylinder also increases, and without the control system, the cantilever rod will deflect. To prevent this deflection, the controller will apply a frequency to the turbine and the fluid. This frequency is obtained by the summation of the two-way structural frequency and the vortex shedding frequency, as shown in Figure 5.

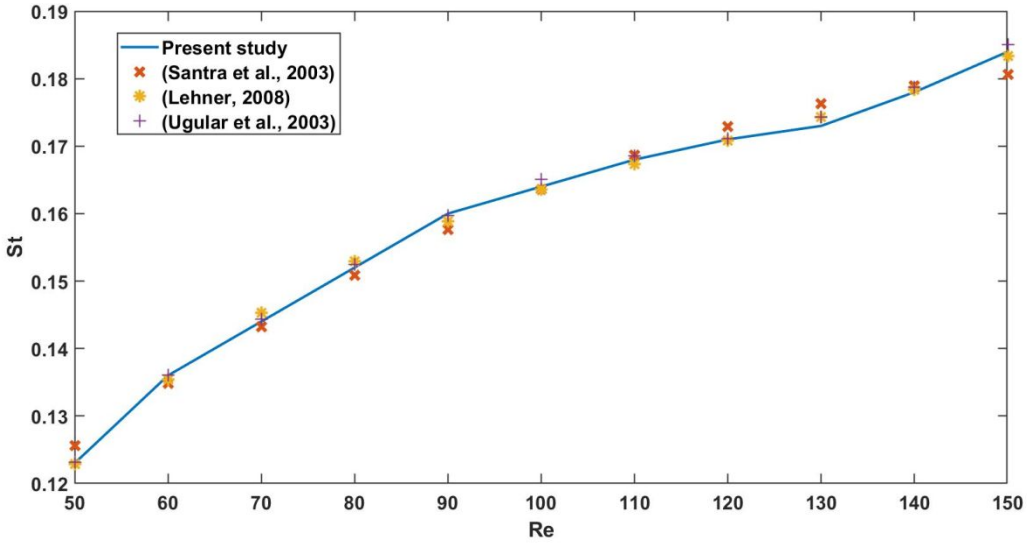


Figure 4. The relation between Strouhal's number and Reynolds number of a fixed cylinder for the present research and validation with four previous studies.

The validation of the relation between the Reynolds and Strouhal dimensionless numbers in the present study using four other studies is shown in Figure 4.

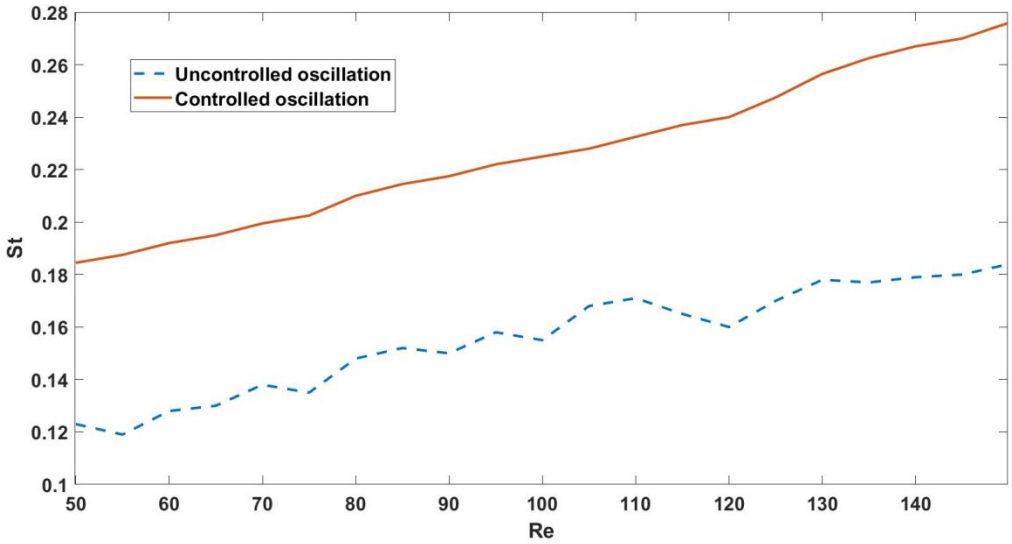


Figure 5. Comparison between the fluid frequency of vortex shedding behind the structure when the system has a controller and when it does not.



By considering the effect of wind velocity on the vorticity of frequency, the Strouhal number indicates the frequency values. As it is observable from Figures 4 and 5, comparing the vorticities and body frequencies, the resonance range will be indicated, where the maximum power happens in this range.

In this study, the lock-on frequency ratio is 1.0, i.e., when the frequency of the turbine motion approaches the flow frequency. When the size and strength of the primary vortex become more significant, the reduction in the length of the produced vortices can be observed more clearly, and the shedding effects take place closer to the turbine body. Then, the vortex energy is converted to mechanical energy of the structure in the form of oscillations. Furthermore, one should consider not only the patterns of vortex formation, but also the flow behavior in this range in order to explain the various flow characteristics.

The variations of Euler dimensionless number with frequency is a key to study the power spectrum. Figure 6 shows the power spectrum of the stream wise velocity behind the bladeless wind turbine without the tuning system, showing that the rod deflection appears earlier. Figure 7 shows this graph with the addition of a tuning system downstream. A comparison of Figures 6 and 7 reveals the effect of the magnetic tuning system in a bladeless turbine. Table 2 shows the change in the Euler number with an increase the frequency for both cases.

Table 2. The relation between the vortex shedding frequency with the Euler dimensionless number with (Eu1) and without (Eu2) a tuning system.

| *f(Hz)* | *0* | *1* | *2* | *3* | *4* | *5* | *6* | *7* | *8* | *9* | *10* | *11* | *12* | *13* | *14* | *15* |
|---|---|---|---|---|---|---|---|---|---|---|---|---|---|---|---|---|
| *Eu1* | 0 | 1/5 | 2 | 3 | 4 | 5 | 10 | 20 | 30 | 50 | 110 | 320 | 400 | 200 | 20 | 0 |
| *Eu2* | 0 | 0.85 | 1.66 | 2.43 | 3.16 | 3.85 | 7.5 | 14.6 | 21 | 34.5 | 71.5 | 195 | 100 | 35 | 0 | 0 |

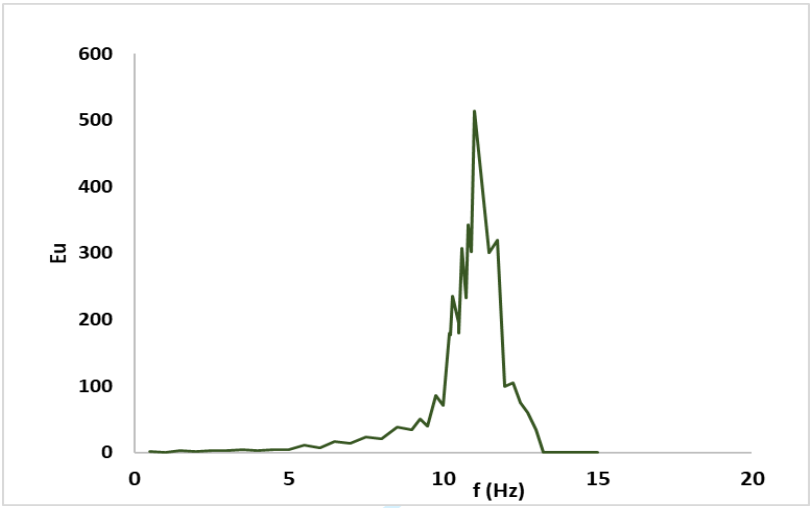


Figure 6. The power spectrum of the stream wise velocity behind a cylinder without a tuning system.

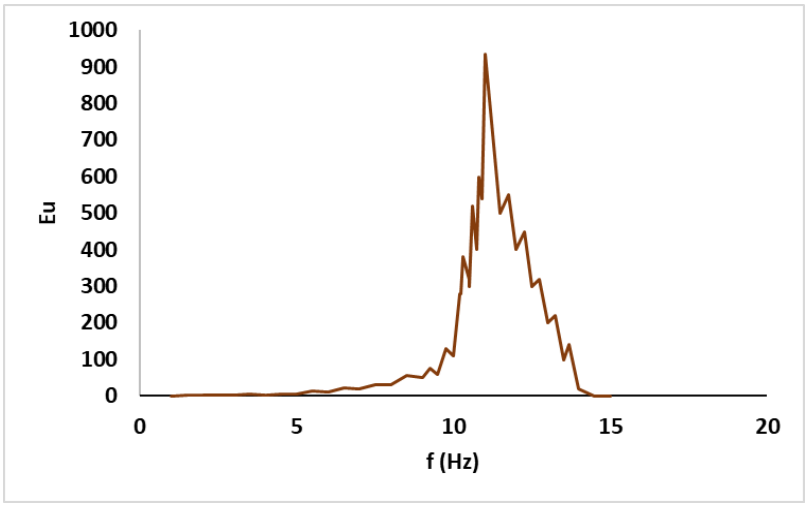


Figure 7. The power spectrum of the stream wise velocity behind an oscillating vortex bladeless wind turbine with a controller.

Furthermore, in the case of the resonant frequency $\eta = 1$, the minimum value of $\frac{U_{mean}}{U_0}$ in this region should be positive (larger than the other frequency ratios and the centerline of the wake $\frac{y}{D} = 0$). The distribution of the velocity ratio with frequency ratios at $\frac{y}{D} = 1$ is plotted in Figure 9. This figure shows that, by considering constant magnitudes for $U_0$ and D, when the height and the diameter of the cylinder are assumed equal ( $\frac{y}{D} = 1$ ), the velocity ratio decreases near the body with the same behavior as behind the cylinder.

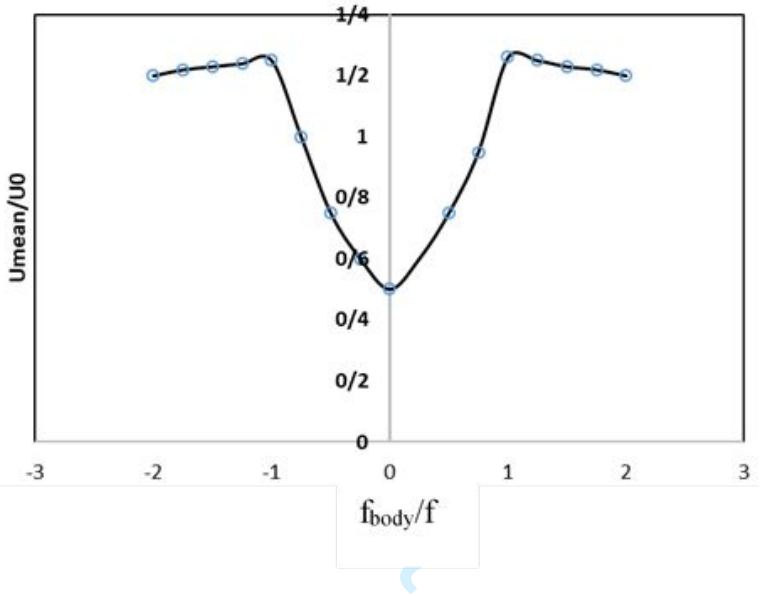


Figure 9. Distribution of the velocity ratio with frequency ratios at $\frac{y}{D} = 1$.

The results show that when the controller is implemented, the power spectrum is much higher. This is because the tuning system regulates the vibrations and increases the velocity of the vortices behind the turbine. Electricity is generated by the turbine.

## 4. Conclusions

The present work addressed the numerical analysis of the VIV phenomenon via CFD method at variable Reynolds numbers ranging from 50 to 150. The first step of the study was to determine the total force applied to the oscillating bladeless wind turbine, which is the result of the drag force and the opposing magnetic force. Results have indicated that it is possible to reduce the vibrations' amplitude, due to the drag force from the magnetic force of the controlling system. It is also observable that the frequency of the moving part of the turbine could be increased then. The next step was an accurate description of the comparison of the frequency in a two

process of a fixed and oscillating cylinder. The simulation results of a cylinder with a semi-circular cross-section forced to vibrate in a direct cross flow were used to compare the different phenomena happening. By considering the effect of St and Re numbers on harvesting energy, the range and amplitude of the vortex shedding frequency have been studied, and also linked together using the free oscillation frequency of the bladeless wind turbine by changing the flow velocity passing the bladeless wind turbine.

The power spectrum of the stream wise velocity behind an oscillating vortex bladeless wind turbine with and without the controller was analyzed. It was found that, when implementing a controller system, the power spectrum was much higher in compare with the case excluding the magnetic controller system and also the rod deflected later when using the tuning system. Furthermore, the Euler number was higher at the same resonant frequency. By utilizing the observations, it can be concluded that when implementing the controller, the efficiency and output power which is produced from bladeless turbine will be increased. As demonstrated, this technology is a suitable option when dealing with low speed winds. A Detailed three-dimensional analysis of vortex-induced vibration could be considered for future research.



## Reference

Arionfard H. and Nishi Y, 2018. Flow-induced vibration of two mechanically coupled pivoted circular cylinders: Vorticity dynamic. J Fluids Struct, **80** (1): 165-178. doi:10.1016/j.jfluidstructs.2018.07.016.

Bai XD, Zhang W. and Wang Y., 2020. Deflected oscillatory wake pattern behind two side-by-side circular cylinders, Ocean Eng, **197** (1): 106847. doi:10.1016/j.oceaneng.2019.106847.

Fekete J.R., and. Hall J.N, 2017. Design of auto body: materials perspective. Automotive Steels, 1–3. doi:10.1016/B978-0-08-100638-2.00001-8.

Gau YY, et al., 2017. Experimental study on flow past a rotating oscillating cylinder. China Ocean Eng, **31** (4) : 495-503. doi:10.1007/s13344-017-0056-8.

Gluck M., et al., 2003. Computation of wind-induced vibrations of flexible shells and membranous structures. J Fluids Struct, **17** (5): 739–765. doi:10.1016/S0889-9746(03)00006-9.

Henderson RD, 1995. Details of the drag curve near the onset of vortex shedding. Phys Fluids, **7**: 2102–4. doi:10.1063/1.868459.

Henderson RD. 1997. Nonlinear dynamics and pattern formation in turbulent wake transition. J Fluid Mech, **352**: 65–112. Available from https://resolver.caltech.edu/CaltechAUTHORS:HENjfm97.

Jiang F., et al., 2017. Flow around an oscillating circular cylinder: Computational issues. JSFM, **16** (8): 1–14. doi:10.1088/1873-7005/aa7e1c.

Klamo JT, et al., 2006. The effects of damping on the amplitude and frequency response of a freely vibrating cylinder in cross-flow. J Fluids Struct, **22** (6): 845–856. doi:10.1016/j.jfluidstructs.2006.04.009.

Lehner G., 2008. Basics of Magnetostatics In: Electromagnetic Field Theory for Engineers and Physicists. Springer, Berlin, Heidelberg. Doi:10.1007/978-3-540-76306-2.

Pham AH, et al., 2010. laminar flow past an oscillating circular cylinder in cross flow. J Mar Sci Technol, **18** (3): 361-368. Available from http://jmst.ntou.edu.tw/marine/18-3/361-368.pdf.

Placzek A., Sigrist JF, and Hamdouni A., 2008. Numerical simulation of an oscillating cylinder in a cross-flow at low Reynolds number: Forced and free oscillations. Comput Fluids, **38** (1): 80-100. doi:10.1016/j.compfluid.2008.01.007.

Rao Z, and Vandiver JK, 2015. Estimation of the Damping Parameter Governing the VIV of Long Flexible Cylinders. Proceedings of the ASME 2015 34th International conference on ocean, offshore and Arctic Engineering (OAME2015), 34, June, pp. 1–3. doi:10.1115/OMAE2015-41296.

Santra T., Et al., 1994. Calculation of Force between Two Ring Magnets Using Adaptive Monte Carlo Technique with Experimental Verification. Prog Electromagn Res, **49** (1): 181-193. doi:10.2528/PIERM16052101.

Ugural, A. C. and Fenster, S. K., 2003. Advanced Strength and Applied Elasticity,4th ed., Prentice-Hall. ISBN 978-0-13-047392-9.

Vandiver JK, 2012. Damping Parameters for flow-induced vibration. Journal of Fluids and Structures, **35**: (6): 105-119. doi:10.1016/j.jfluidstructs.2012.07.002.

Wang H., Zhai Q. and Jisheng Zhang, 2018. Numerical study of flow-induced vibration of a flexible plate behind a circular cylinder, Ocean Eng, **163** (1) 419-430. doi:10.1016/j.oceaneng.2018.06.004.

Yanez Villarreal DJ, 2018. VIV resonant wind generators. European Union's Horizon 2020 research and innovation program under grant agreement No 726776. Available from URL http://www.vortexbladeless.com.